Research Signpost
Trivandrum
Kerala, India

Recent Advances in Pharmaceutical Sciences VII, 2017: 83-100 ISBN: 978-81-308-0573-3
Editors: Diego Muñoz-Torrero, Montserrat Riu and Carles Feliu

6. Deciphering the stack, a novel bacterial structure, by (cryo-) transmission electron microscopy and (cryo-) electron tomography

Lidia Delgado[1], Carmen López-Iglesias[2] and Elena Mercadé[3]
[1]Cryo-Electron Microscopy Unit, Scientific and Technological Centers, University of Barcelona, Barcelona, Spain; [2]The Institute of Nanoscopy, Maastricht University, 6211 LK, Maastricht, The Netherlands [3]Department of Biology, Health and Environment, Faculty of Pharmacy and Food Sciences, University of Barcelona, Barcelona, Spain

Abstract. The recent development of cryo-electron microscopy and cryo-electron tomography has allowed prokaryotic cells to be studied in a close-to-native state, refining our knowledge of already known structures and enabling new ones to be discovered. Their application to the Antarctic cold-adapted bacterium *Pseudomonas deceptionensis* $M1^T$ revealed the existence of a novel cytoplasmic structure called a "stack", which to date has been visualized mainly in slow-growing cultures of *P. deceptionensis* $M1^T$. The stack appears as a set of stacked oval discs, variable in number, surrounded by a lipid bilayer. Found in the bacterial cytoplasm in varying amounts, stacks are located close to the cell membrane and to DNA fibers. Stacks were also visualized in slow-growing cultures of other bacteria and may play a role in the chromosome dynamics.

Correspondence/Reprint request: Dr. Elena Mercadé, Laboratory of Microbiology, Faculty of Pharmacy and Food Sciences, University of Barcelona, Barcelona, Spain. E-mail: mmercade@ub.edu

Introduction

For many years, the prokaryote cytoplasm was thought to be a homogeneous compartment containing macromolecules and few structures of interest compared to eukaryotic cells. In most prokaryotes, when the cytoplasm was visualized by conventional transmission electron microscopy (TEM), it was only possible to observe irregular areas of fibrous appearance corresponding to the nucleoid, and numerous small granules scattered throughout the rest of the cytoplasm, which are the ribosomes [1]. In some prokaryotes, inclusions and vesicles involved in several physiological processes were also observed [2], [3], [4], [5], [6], [7], [8].

Recent improvements in TEM have enhanced our knowledge of bacterial ultrastructure, and prokaryotes have been reappraised as organized assemblies of macromolecular machines [9] optimized to travel through and interact with complex and dynamic environments [10]. The task of deciphering the structure, function and spatial organization of molecular machines inside the fluid architecture of bacterial cells has emerged as a new challenge [10], [11], [12].

Cryo-electron microscopy (Cryo-EM) combined with electron tomography (ET) provides the highest available resolution for the imaging of biological specimens. These "pure" cryo-techniques have revealed cellular organelles and macromolecular assemblies in frozen-hydrated close-to-native samples. Importantly, they avoid the traditional preparation methods for TEM that involve treating samples with chemical fixatives, organic solvents, contrast-enhancing staining solutions, and resins, which can denature structures and introduce misleading artifacts [13], [14]. This is achieved by very high cooling rates that turn the intrinsic water of cells into vitreous ice, avoiding crystal formation and phase segregation between water and solutes [15]. One way to obtain the cooling rates required for water vitrification is the plunge-freezing method, in which 'whole-mount' plunge-frozen specimens are embedded in a thin film of vitreous ice, preserving their native cellular structures. The specimens can be imaged directly when their thickness is below 0.5 μm, a range that includes many bacteria and archaea [16], [17], [18], [19], [20], [21], [22], [23], [24], [25], [26], [27]. However, the Cryo-EM resolution of plunge-frozen whole bacteria is conditioned by the width of the sample, which in the worst of cases can limit the observation of macromolecular details.

Cryo-electron microscopy of vitreous sections (CEMOVIS) is an alternative technique to study frozen-hydrated bacteria and offers better resolution than the observation of whole-mount bacteria by plunge-freezing. It starts with high-pressure freezing (HPF), which can vitrify samples up to 200 μm by increasing the pressure to 2,048 bars during a cooling process of a few milliseconds. These conditions allow the water to become denser than liquid water (vitreous ice), and prevent ice crystal formation [15]. Ultrathin vitreous sections can be obtained directly from high-pressure frozen bacteria and imaged in the microscope, revealing macromolecular details such as the lipid bilayer membrane [28], [29]. However, it is important to bear in mind that the mechanical action of cutting can add conspicuous artifacts to the sample, so a correct interpretation is crucial [30].

Frozen-hydrated specimens can be processed by cryo-electron tomography (CET), which consists in producing a three-dimensional image of a solid object, allowing sectioning of the reconstructed volume and imaging of its internal structures. Tomography is performed by incrementally tilting the sample in the Cryo-EM through a range up to ±70 and it is imaged at each step. Afterwards, the tilt series of images is aligned and processed to generate a 3D reconstruction or tomogram of the specimen at a macromolecular resolution (around 4 nm). The limited tilt range in electron tomography results in a region empty of information in the Fourier space of the 3D reconstruction, referred to as the missing wedge. The resulting artifacts include blurring of the spatial features in the beam direction, which can result in 22% loss of information [31].

CET has been applied to previously characterized frozen-hydrated assemblies, providing new information and a greater understanding of the complex ultrastructure of prokaryotic cells in their natural context. This has given new insights into various aspects of prokaryotic physiology, including metabolism, interspecies cooperation and pathogenesis [10]. Furthermore, the use of Cryo-EM and CET has opened up fresh opportunities for discovering novel bacterial features, partly because new bacterial species are being analyzed, but also thanks to the improvements in sample preparation and gains in resolution [32], [33].

1. The stack, a novel bacterial structure

The stack was first visualized in the Antarctic bacterium *Pseudomonas deceptionensis* M1^{T}. The strain was isolated from marine sediment collected

on Deception Island and was described as rod-shaped (cell length: 1.5-2 μm; cell diameter: 0.5 μm), catalase- and oxidase-positive, motile by means of a polar flagellum and psychrotolerant (able to grow at temperatures ranging from -4 to 34ºC) [34]. With the aim of characterizing its ultrastructure, the strain was grown on different media, varying the time and temperature. Afterwards, cells were cryo-immobilized by HPF and processed by freeze-substitution (FS), Epon embedding and sectioning. The TEM analysis of the 60-nm Epon sections revealed a highly organized stacked structure located in the bacterial cytoplasm, which was unlike any cytoplasmic inclusion or structure reported to date. Interestingly, stacks have only been frequently observed in *P. deceptionensis* $M1^T$ cells grown under specific slow-growth conditions, such as low incubation temperatures: on trypton soy agar (TSA) plates, for 12 days at 0ºC. Under these growth conditions, 23.23% of the cells analyzed by TEM showed stacks in their cytoplasm. The frequent observation of stacks at 0ºC may be associated with the slow growth of the strain at this temperature, which may prolong dynamic processes and make it easier to capture the temporary structures involved. In that case, stacks might be dynamic cytoplasmic structures required to localize certain molecules or enzymes in a particular place and cellular moment for a particular cellular function. Consequently, stacks may be quickly assembled where their function is required, to be then dismantled once their function is fulfilled [35], [1].

Semithin Epon sections of 250 nm of *P. deceptionensis* $M1^T$ cells grown on TSA at 0ºC for 12 days and processed by HPF-FS and Epon embedding were further explored three-dimensionally by ET. Dual-axis tilt series from the 250 nm Epon sections were acquired in the TEM at 200 kV, each tilt series being reconstructed using Tomo3D software. Tomograms corresponding to each series were combined with the IMOD software and the final dual-axis tomogram was obtained. Figure 1 shows the XY, ZY and XZ tomogram slices from the same point (marked by an asterisk in the different views) of the double-axis tomogram, and two views of its segmentation (B and C). The XY view in Figure 1A (top left image) clearly shows two contiguous stacks at an angle of 130º to each other. Both are located near the boundaries of the cell plasma membrane (PM) and the one on the left is perpendicular to the PM. In the YZ view, the stack appears as a pile of flat structures oriented perpendicularly to the surface (top right image). The XZ view (bottom left image) shows two oval structures, which correspond to the frontal views of two flat discs. The tomogram segmentation from the dual-axis tomogram observed in Figures 1B and 1C confirm the presence of two contiguous stacks, one on the right and the other on the left, formed by parallel oval discs [1].

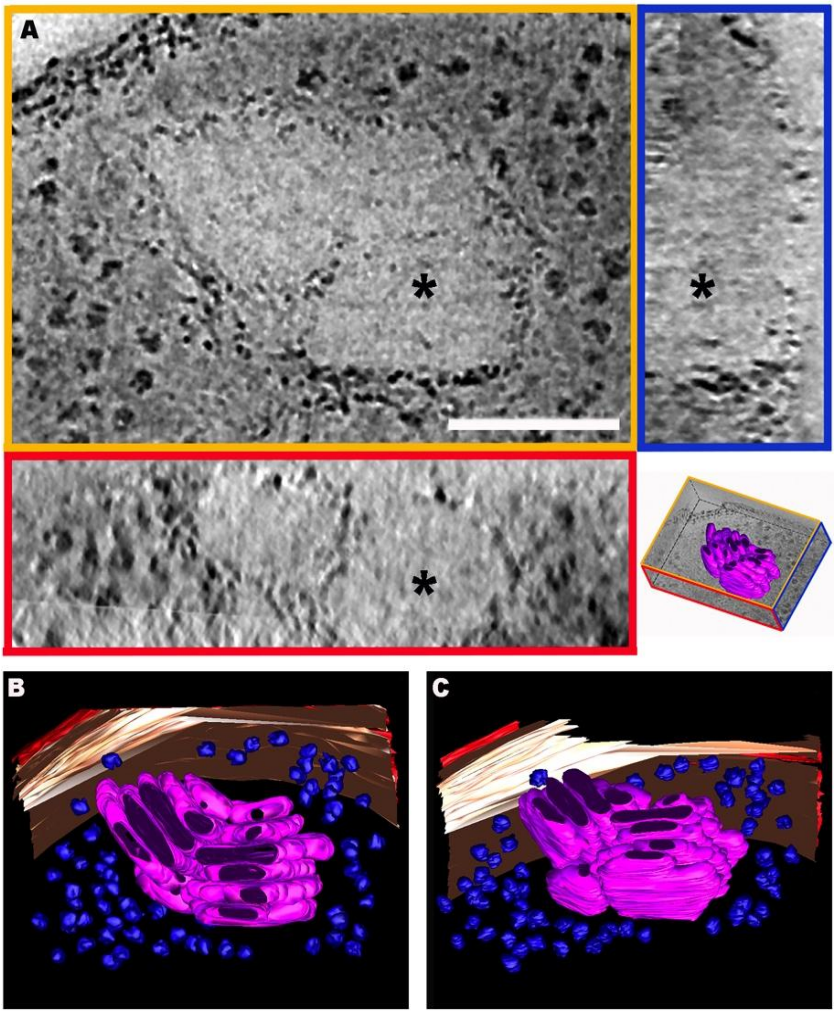

Figure 1. 3D visualization of stacks observed in *P. deceptionensis* $M1^T$ cells after HPF-FS [1]. (A) 2 nm tomogram slices from the XYZ views of a tomogram reconstructed from a 250 nm Epon section. The asterisks correspond to the same point through the different views. Scale bar = 100 nm. The bottom right picture depicts the view distribution in the tomogram. (B-C) Two different views from the segmentation of the tomogram observed in (A). In red, the outer membrane; in cream-color, the PM; in blue, the ribosomes; and in pink, the discs.

Based on the data obtained, the stack was defined as a pile of oval-disc-shaped subunits surrounded by a membrane structure (from 1 to 14 discs per stack) localized in the bacterial cytoplasm. They were frequently found very near the PM, mostly very close to DNA fibers, and in variable number within each cell (1 to 4 stacks per cell, simultaneously). When more than one stack was observed simultaneously in the cytoplasm, they appeared isolated or grouped/contiguous [1]. Three-dimensionally, each subunit appeared as a flat oval disc, while in 2D views, the stack had either an oval structure or appeared as a pile of sticks (Fig. 2).

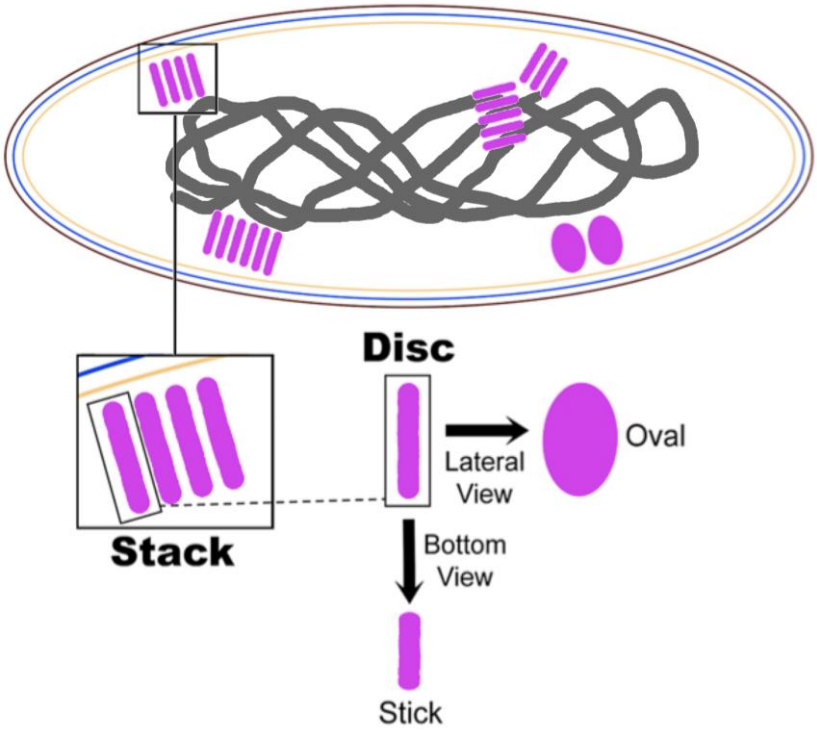

Figure 2. Model of a *Pseudomonas deceptionensis* M1^T cell showing stacks in the cytoplasm (adapted from [36]). Lateral and front views of the squared subunit are shown. In 2D views, the disc-shaped subunit of the stack can be observed as an oval structure or as a stick. Pink: stacks; grey: nucleoid; red: outer membrane; blue: peptidoglycan layer; cream-color: plasma membrane.

2. Stacks in the whole-cell context

With the aim of increasing knowledge of the architecture and spatial organization of stacks inside the cytoplasm, plunge-frozen whole

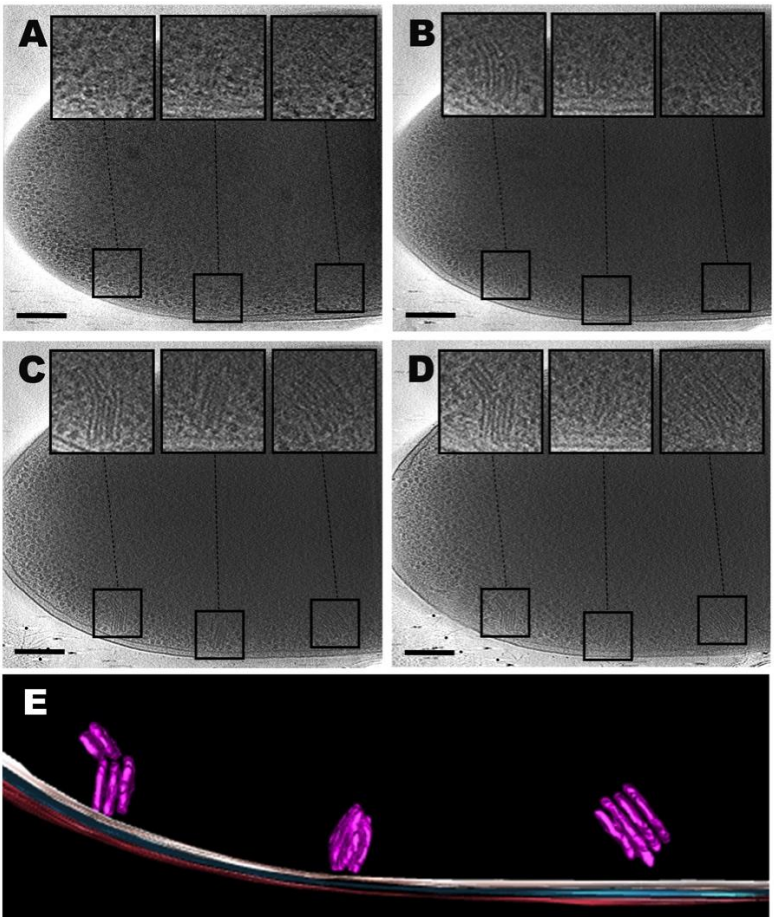

Figure 3. Stacks analyzed by CET of plunge-frozen whole bacteria. (A-D) 2-nm slices of a tomogram reconstructed from a plunge-frozen *P. deceptionensis* $M1^T$ cell. Objective lens defocus: -6 µm. Pixel size: 0.85 nm. (E) Partial segmentation of the tomogram observed in (A-D). Pink: stacks; Red: outer membrane; Blue: peptidoglycan layer; Cream-color: PM. Scale bars = 200 nm.

P. deceptionensis M1^T cells were imaged by Cryo-TEM. Stacks were revealed in the peripheral regions of the bacteria, verifying that they were not artifacts derived from the previous preparation methods (Fig. 3A-D). They were only visible in areas thin enough to allow an electron beam to pass through, namely the peripheral areas of the cell. Measurements of the length and width of stack subunits in images with a pixel size of 0.81 nm provided the mean values of 90.7±25 nm and 13.3±1.7 nm, respectively. While the length of the discs was distinctly variable, the width was practically constant. It should be noted that the discs were separated by an apparently constant distance (5.2±1.3 nm), although no spacing features were observed between them. Cryo-tomograms showed the stacks located at the inner perimeter of the *P. deceptionensis* M1^T cells and angled at 35 to 90º with respect to the PM. Figure 3E depicts the stack segmentation observed in the tomogram slices in Figures 3A-D [36].

Analysis of plunge-frozen bacteria also showed that each stack subunit was clearly delimited by an electron-dense layer resembling a lipid membrane, but no continuity between this layer and the PM was observed in the whole tomograms. Measurements of the width of the membrane-like layers surrounding these subunits and the width of the PM provided the mean values 4.2±0.8 nm and 6±1.1 nm, respectively. Analysis of the measurements by the one-factor ANOVA test gave a p-value < 0.0001, and revealed significant differences between the widths of the two membrane types, suggesting differing composition or structure. Taken as a whole, these data indicate that stacks are not invaginations of the PM [36].

3. Nature of the membrane surrounding the stack subunits

To shed more light on the composition of the membrane surrounding the stack discs, 50-nm vitreous sections (VIS) of high-pressure frozen *P. deceptionensis* M1^T cells were analyzed by cryo-TEM, a technique that provides a better resolution than the study of plunge-frozen whole specimens (Fig. 4A and 4B). Depending on the orientation of the VIS with respect to the cells, the lipid bilayer pattern of the PM was observed, as well as a typical two-peak density profile (Fig. 4B, see squared area). The layer delimiting each stack subunit presented a similar electron density to the PM, although no bilayer pattern was discernible (Fig. 4A and 4B) [36].

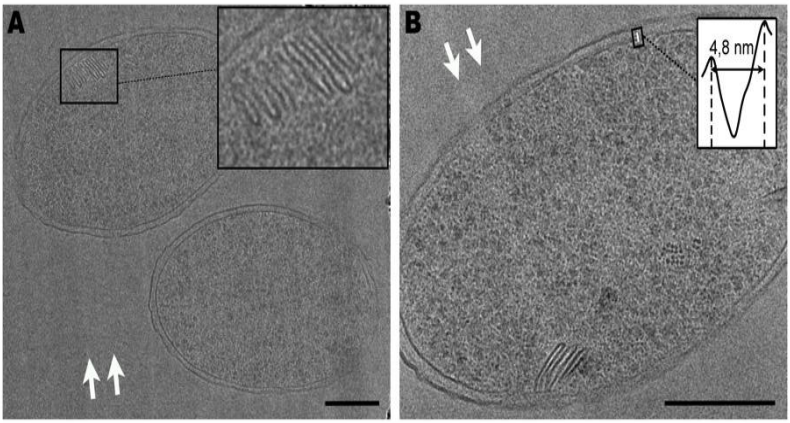

Figure 4. Cryo-TEM visualization of stacks in *P. deceptionensis* M1^T [36]. (A-B) 50-nm VIS. (B) The density profile of a section of the PM is observed in the squared area confirming the lipid bilayer pattern. White arrows indicate the cutting directions. Scale bars = 200 nm.

Cryo-electron tomography of vitreous sections (CETOVIS) was then carried out, recording tilt series of images from -60º to +60º. The subsequent 4-nm resolution tomograms revealed that through the z-axis the stacks were composed of discs clearly delimited by membrane-like structures (Fig. 5A and 5C). Additionally, analysis of tomograms obtained from VIS revealed a lipid bilayer membrane pattern in the layer surrounding each disc (Fig. 5A see magnified area), which was confirmed by the density profile (Fig. 5A). It was notable that when stacks were observed in VIS tomograms, the PM lipid bilayer was frequently not resolved. As stacks are localized in the peripheral regions of the bacterial cytoplasm, the section cutting may occur away from the central plane. Consequently, the membrane is not cut perpendicularly and the overlapping head group regions obliterate the gap of the bilayer structure, thus obscuring visualization of the membrane bilayer pattern. Since the stacks appeared clearly delimited throughout the z-axis, more reliable segmentations of the structures were obtained (Fig. 5B and 5D) [36].

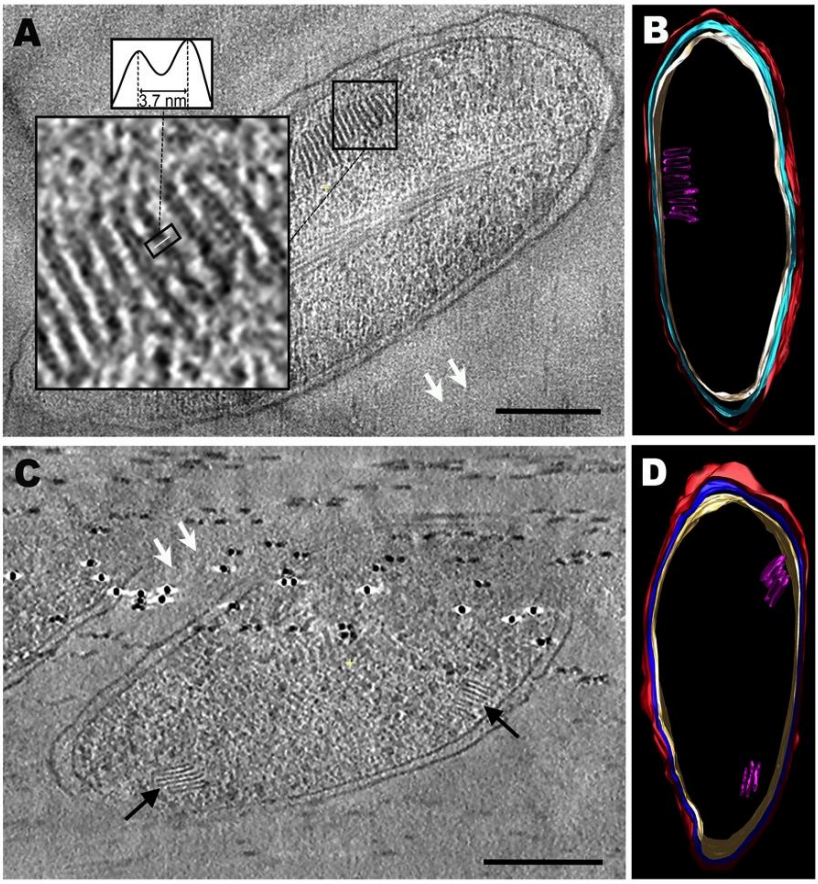

Figure 5. Stacks analyzed by CETOVIS [36]. (A and C) 1-nm slices of tomograms reconstructed from 50 nm vitreous sections of *P. deceptionensis* M1^T. Objective lens defocus: -6 µm. Pixel size: 0.71 nm. (A) The magnified square shows a fragment of one stack with subunits surrounded by a membrane-like structure exhibiting the typical pattern of a lipid bilayer membrane. The density profile of a section of the membrane-like structure surrounding the discs is observed in the upper squared area, revealing the typical two peaks of a lipid bilayer membrane. (C) Two stacks are observed isolated in different positions within the cytoplasm of the bacterial cell. (B and D) Segmentations of the tomograms observed in (A) and (C), respectively. Pink: stacks; red: outer membrane; Blue: peptidoglycan layer; Cream-color: PM. White arrows indicate the cutting direction. Scale bars = 200 nm.

4. Stack localization and the bacterial nucleoid

Interestingly, stacks observed near the periphery of HPF-FS Epon-embedded cells grown at 0ºC for 12 days frequently appeared very close to DNA microfibers from the nucleoid (Fig. 6A), in some cases

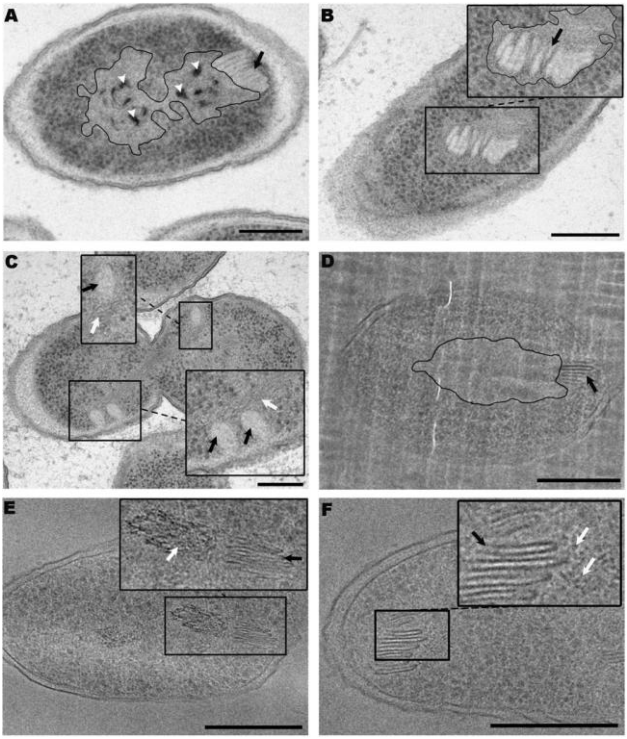

Figure 6. Stacks and DNA location in *P. deceptionensis* $M1^T$ cells [1]. (A-C) TEM micrographs of 60 nm Epon sections of samples processed by HPF-FS. (A) Stack (black arrow) perpendicular to the plasma membrane and very close to the bacterial nucleoid (outlined area). The bacterial nucleoid shows poly P granules (white arrow heads). (B) Stack (black arrow) embedded in the nucleoid area (outlined area). (C) Dividing cell distributing its DNA among its daughter cells; stacks very close to the DNA microfibers (white arrows). (D-F) CEMOVIS micrographs. (D) Stack (black arrow) very close to a RFA or nucleoid area (outlined area). (E) Stack (black arrow) in the vicinities of a locally ordered arrangement of DNA microfibers (white arrow). (F) Stack (black arrow) very close to DNA microfibers (white arrows). Scale bars = 250 nm.

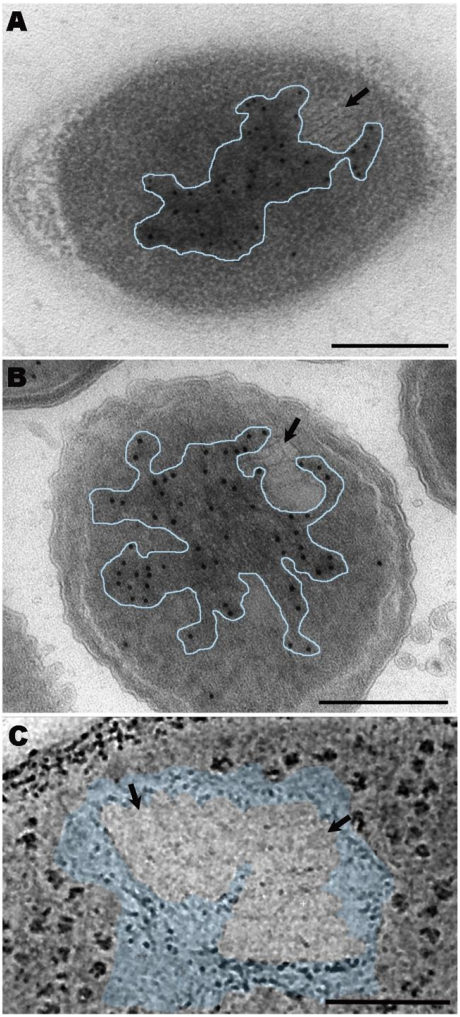

Figure 7. TEM studies analyzing the proximity between stacks and DNA *P. deceptionensis* M1^{T} [1]. (A) DNA immunolabeling on 60-nm HM23 Lowicryl sections from HPF-FS-processed samples. (B) DNA immunolabeling on a 60 nm section obtained by Tokuyasu´s method. (A-B) Black arrows indicate stacks and outlined areas correspond to the nucleoid. (C) 2-nm tomogram slice of a tomogram reconstructed from a 250 nm Epon section of a HPF-FS-processed sample. Black arrows indicate stacks and the colored area corresponds to the nucleoid. Scale bars = 250 nm.

being completely embedded (Fig. 6B). Cells dividing and distributing their DNA among daughter cells also showed stacks very close to the DNA fibers (Fig. 6C). Additionally, inorganic polyphosphate (Poly P) granules, commonly observed in nucleoid areas, were frequently located very near to stacks (Fig. 6A, white arrow heads) [1].

The same proximity between DNA and stacks described in Epon sections was also observed in VIS. Stacks were localized next to ribosome-free areas (RFA) corresponding to the bacterial nucleoid (Fig. 6D). Locally ordered arrangements of DNA and DNA microfibers were also visualized very close to stacks (Fig. 6E and Fig. 6F) [1].

DNA immunolabeling and tomographic studies performed on samples of *P. deceptionensis* $M1^T$ TSA-grown at 0ºC for 12 days confirmed the co-localization of stacks and DNA. Immunolabeling experiments were performed in HM23 and Tokuyasu sections using a specific antibody for labeling double-stranded DNA. In the HM23 sections, we also amplified the signal obtained with a DNA staining method using potassium permanganate, which allows the chromatin distribution within the bacterial cytoplasm to be visualized. The micrographs again revealed stacks at the periphery of the bacterial cytoplasm, contiguous with or partially embedded in DNA microfibers (Fig. 7A and Fig. 7B). ET of Epon sections of *P. deceptionensis* $M1^T$ cells showed stacks completely embedded in the bacterial nucleoid along the whole Z-axis (Fig. 7C) [1].

The frequent co-localization of the stacks and the bacterial nucleoid suggest a possible relationship between these new structures and certain processes involved in the bacterial chromosome dynamics. Further experiments are needed to explore this hypothesis [1].

5. Stacks in other bacterial species

The frequent presence of stacks very close to DNA microfibers suggests they could play a role in the bacterial chromosome dynamics, in which case their presence would not be limited to the *P. deceptionensis* $M1^T$ strain. We therefore chose three bacterial species within the *Pseudomonas* genus, two of which, *P. psychrophila* DSM 17535^T and *P. fragi* DSM 3456^T, are closely related to *P. deceptionensis* $M1^T$, while the third, *P. fluorescens* ATCC 13430^T, is phylogenetically more distant. All the strains were grown on TSA plates for 12 days and the range of growth temperatures was determined for each species in order to reproduce slow-growing conditions. The samples

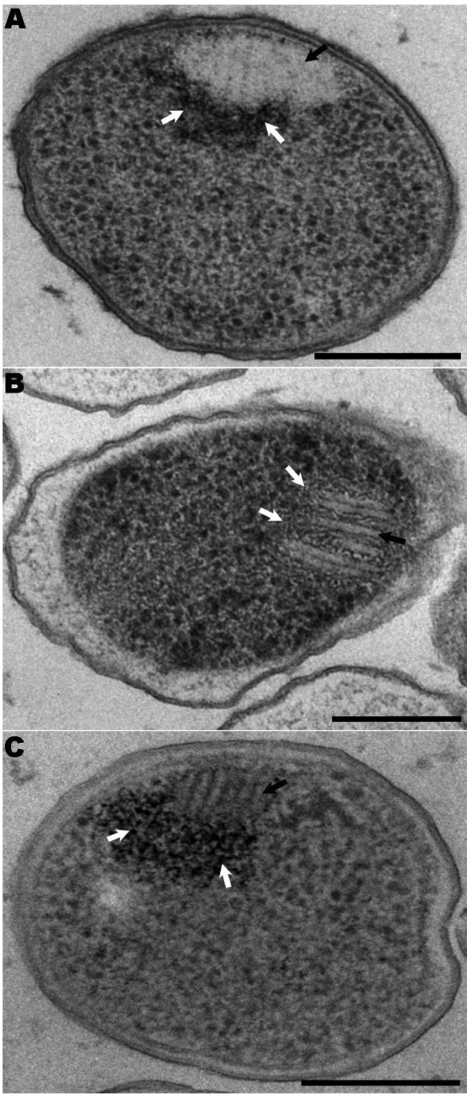

Figure 8. Stacks visualized in different *Pseudomonas* species from samples processed by HPF-FS [1]. (A-C) 60 nm Epon sections. (A) *P. psychrophila* DSM 17535^T TSA-grown culture. (B) *P. fragi* DSM 3456^T TSA-grown culture. (C) *P. fluorescens* ATCC 13430^T TSA-grown culture. (A-C) Black arrows indicate stacks and white arrows DNA microfibers. Scale bars = 250 nm.

were then processed by HPF-FS and Epon-embedding and imaged by TEM. Micrographs revealed that *P. psychrophila* DSM 17535^T and *P. fragi* DSM 3456^T incubated at 0ºC, and *P. fluorescens* ATCC 13430^T incubated at 4ºC all presented stacks in their cytoplasms. In these three strains, stacks were also found perpendicular to the PM, and close to DNA microfibers presenting inorganic polyphosphate, as described for *P. deceptionensis* M1^T (Fig. 8A, 8B and 8C) [1].

These results confirmed that stacks are not exclusive to the Antarctic bacterium *P. deceptionensis* M1^T, having been visualized in other species of the *Pseudomonas* genus, where they were structurally very similar and observed only in slow-growing cells, and close to DNA microfibers [1].

Other bacteria genera were studied to determine if the presence of this new bacterial feature was limited to species within the *Pseudomonas* genus. Two bacterial model species were selected: *Escherichia coli* W3310 and *Bacillus subtilis* ATCC6633. The presence of stacks in these species would help to determine their possible implication in the chromosome dynamics, thanks to the availability of molecular tools to study this process in these model species. Both strains were grown on TSA plates for 12 days and the range of growth temperatures was determined in order to reproduce slow-growing conditions (12ºC). The samples were then processed by HPF-FS and Epon-embedding and imaged by TEM. Both strains revealed structures with a morphology, size and location indicative of stacks, but the subunits were not as clearly defined (Fig. 9). Although the data suggested that stacks might be present in other bacterial genera, further experiments are needed to determine the optimum growing conditions in the studied strains for an improved visualization before the hypothesis can be confirmed [35].

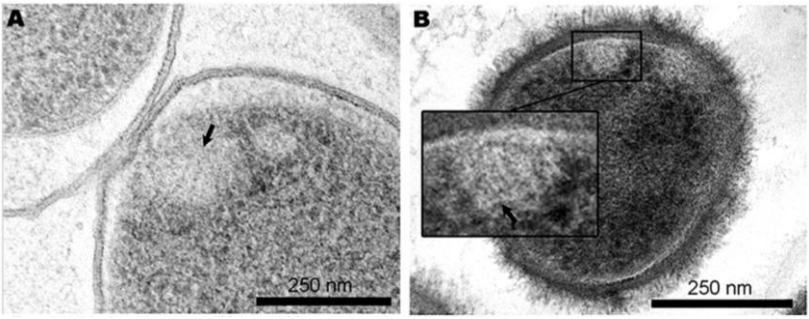

Figure 9. Stack-like structures visualized in *E. coli* W3310 (A) and *B. subtilis* ATCC6633 (B) processed by HPF-FS [35]. (A-B) 60 nm Epon sections. Black arrow and black squares highlight the stack-like structures.

6. Conclusion

Applying cryo-TEM techniques to study the Antarctic bacterium *P. deceptionensis* $M1^T$ and other bacteria in slow-growing conditions has led to the discovery of a new cytoplasmic structure, termed a stack. This new bacterial feature can be described as a set of stacked discs surrounded by a lipid bilayer with a different composition from that of the PM. It is usually located at the boundaries of the cell cytoplasm, close to the PM and possibly not continuous with it, and frequently near the bacterial DNA microfibers, suggesting a possible role in the chromosome dynamics.

The combination of CET of plunge-frozen whole bacteria and CETOVIS has proved useful in providing reliable structural information about these new bacterial cytoplasmic structures at different resolutions and in a general cellular context.

Acknowledgements

The authors are grateful to Dr. Peter Peters and Dr. Jason Pierson (NKI-AVL) for their help to develop vitreous cryo-sectioning in our lab, to Dr. José Jesús Fernández (CNB) and to Dr. José María Seguí (COMAV) for their help to develop in tomography and 3D reconstructions in our lab, and Dr. Martin Rios (UB) for his statistical support. This work received funding from the following sources: grant CTQ2014-59632-R from the Ministerio de Economia y Competitividad, Spain; and grant 2014SGR1325 from the Departament d'Innovació, Universitats i Empresa from the Autonomous Goverment of Catalonia.

References

1. Delgado, L., Carrión, O., Martínez, G., López-Iglesias, C., Mercadé, E. 2013, *PLoS One*, Sep 9;8(9):e73297. doi:10.1371/journal.pone.0073297.
2. Walsby, A.E. 1994, *Microbiol. Rev.*, 58, 94.
3. Shively, J.M., Ball, F., Brown, D.H., Saunders, R.E. 1973, *Science*, 584.
4. Parsons, J.B., Dinesh, S.D., Deery, E., Leech, H.K., Brindley, A.A., Heldt, D., et al. 2008, *J. Biol. Chem.*, 283, 14366. doi:10.1074/jbc.M709214200.
5. O'Connell, J.D., Zhao, A., Ellington, A.D., Marcotte, E.M. 2012, *Annu. Rev. Cell Dev. Biol*. 28: 89. doi:10.1146/annurev-cellbio-101011-155841.
6. Shively, J.M. 1974, *Annu. Rev. Microbiol*., 28, 167. doi:10.1146/annurev.mi.28.100174.001123.
7. Bazylinski, D.A., Frankel, R.B. 2004, *Nat. Rev. Microbiol*., 2, 217. doi:10.1038/nrmicro842.

8. Niederman, R.A. in: Shively, J.M., editor 2006, *Springer Berlin Heidelberg*, 193–227. http://link.springer.com/chapter/10.1007/7171_025.
9. Alberts, B. 1998, *Cell*, 92, 291. doi:10.1016/S0092-8674(00)80922-8.
10. Oikonomou, C.M., Jensen, G.J. 2016, *Nat. Rev. Microbiol*., 14, 205. doi:10.1038/nrmicro.2016.7.
11. Gitai, Z. 2005, *Cell*, 120, 577. doi:10.1016/j.cell.2005.02.026.
12. Milne, J.L.S., Subramaniam, S. 2009, *Nat. Rev. Microbiol*., 7, 666. doi:10.1038/nrmicro2183.
13. Pilhofer, M., Ladinsky, M.S., McDowall, A.W., Jensen, G.J. 2010, *Methods Cell. Biol.*, 96, 21. doi:10.1016/S0091-679X(10)96002-0.
14. Pilhofer, M., Aistleitner, K., Ladinsky, M.S., König, L., Horn, M., Jensen, G.J. 2014, *Environ. Microbiol.*, 16: 417–429. doi:10.1111/1462-2920.12299.
15. Studer, D., Humbel, B.M., Chiquet, M. 2008, *Histochem. Cell Biol.*, 130: 877. doi:10.1007/s00418-008-0500-1.
16. Beeby, M., Cho, M., Stubbe, J., Jensen, G.J. 2012, *J. Bacteriol*., 194, 1092. doi:10.1128/JB.06125-11.
17. Toso, D.B., Henstra, A.M., Gunsalus, R.P., Zhou, Z.H. 2011, *Environ. Microbiol.*, 13, 2587. doi:10.1111/j.1462-2920.2011.02531.x.
18. Kudryashev, M., Cyrklaff, M., Wallich, R., Baumeister, W., Frischknecht, F. 2010, *J. Struct. Biol.*, 169, 54. doi:10.1016/j.jsb.2009.08.008.
19. Comolli, L.R., Baker, B.J., Downing, K.H., Siegerist, C.E., Banfield, J.F. 2008, *ISME J.*, 3, 159. doi:10.1038/ismej.2008.99.
20. Khursigara, C.M., Wu, X., Subramaniam, S. 2008, *J. Bacteriol*. 190, 6805. doi:10.1128/JB.00640-08.
21. Murphy, G.E., Matson, E.G., Leadbetter, J.R., Berg, H.C., Jensen, G.J. 2008, *Mol. Microbiol.*, 67, 1184. doi:10.1111/j.1365-2958.2008.06120.x.
22. Li, Z., Trimble, M.J., Brun, Y.V., Jensen, G.J. 2007, *EMBO J.*, 26, 4694. doi:10.1038/sj.emboj.7601895.
23. Zhang, P., Khursigara, C.M., Hartnell, L.M. 2007, *Proc. Natl. Acad. Sci. U.S.A.*, 104, 3777. doi:10.1073/pnas.0610106104.
24. Briegel, A., Dias, D.P., Li, Z., Jensen, R.B., Frangakis, A.S., Jensen, G.J. 2006, *Mol. Microbiol.*, 62, 5. doi:10.1111/j.1365-2958.2006.05355.x.
25. Comolli, L.R., Kundmann, M., Downing, K.H. 2006, *J. Microsc.*, 223, 40. doi:10.1111/j.1365-2818.2006.01597.x.
26. Komeili, A., Li, Z., Newman, D.K., Jensen, G.J. 2006, *Science*, 311, 242. doi:10.1126/science.1123231.
27. Scheffel, A., Gruska, M., Faivre, D., Linaroudis, A., Plitzko, J.M., Schüler, D. 2006, *Nature*, 44,: 110. doi:10.1038/nature04382.
28. Hoffmann, C., Leis, A., Niederweis, M., Plitzko, J.M., Engelhardt, H. 2008, *Proc. Natl. Acad. Sci.* 105, 3963. doi:10.1073/pnas.0709530105.
29. Zuber, B., Chami, M., Houssin, C., Dubochet, J., Griffiths, G., Daffé, M. 2008, *J. Bacteriol*., 190, 5672. doi:10.1128/JB.01919-07.
30. Al-Amoudi, A., Studer, D., Dubochet, J. 2005, *J. Struct. Biol.*, 150, 109. doi:10.1016/j.jsb.2005.01.003.
31. Fernández, J.J. 2012, *Micron*, 43, 1010. doi:10.1016/j.micron.2012.05.003.

32. Moissl, C., Rachel, R., Briegel, A., Engelhardt, H., Huber, R. 2005, *Mol. Microbiol*., 56, 361. doi:10.1111/j.1365-2958.2005.04294.x.
33. Shetty, A., Chen, S., Tocheva, E.I., Jensen, G.J., Hickey, W.J. 2011, *PLoS ONE*, 6: e20725. doi:10.1371/journal.pone.0020725.
34. Carrión, O., Miñana-Galbis, D., Montes, M.J., Mercadé, E. 2011, *Int. J. Syst. Evol. Microbiol.*, 61, 2401. doi:10.1099/ijs.0.024919-0.
35. Delgado, L. 2015, http://diposit.ub.edu/dspace/handle/2445/63070.
36. Delgado, L., Martínez, G., López-Iglesias, C., Mercadé, E. 2015, *J. Struct. Biol.* 189,220. doi:10.1016/j.jsb.2015.01.008.